Supporting Information

Interfacial architecting with anion treatment for enhanced thermoelectric power of flexible ternary polymer nanocomposites

Jiaqian Zhou, Peng Peng, Zhao Li, Lirong Liang, Xuan Huang, Haicai Lv, Zhuoxin Liu and Guangming Chen**

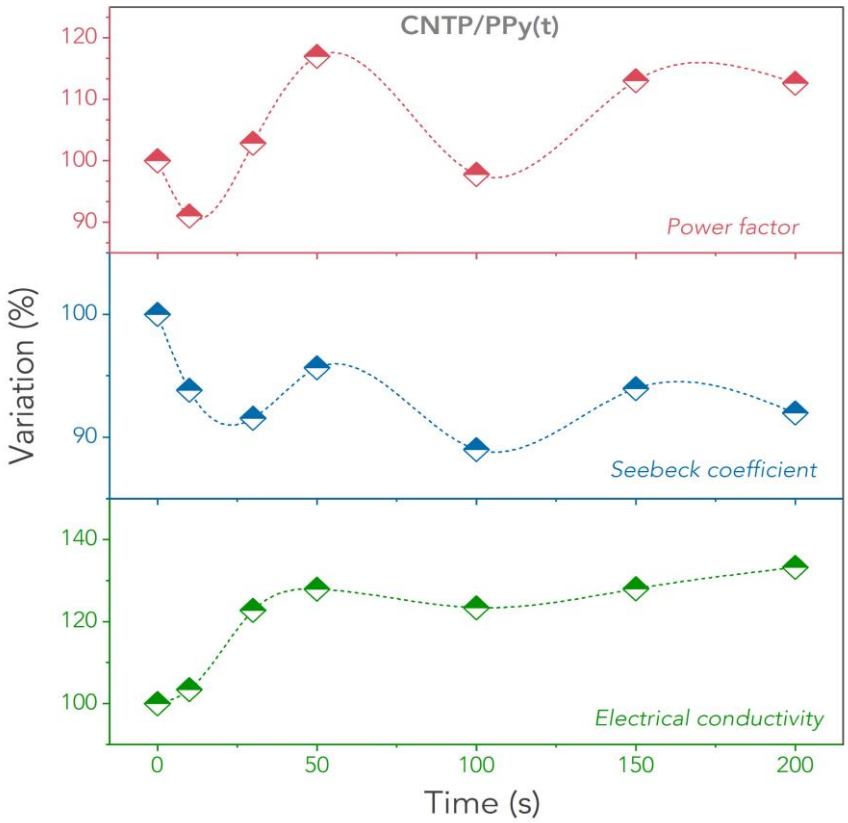

Figure S1. TE property variation as a funtion of electrochemical deposition time of PPy for the CNTP/P_y composites. The reference data (100%) is extracted from CNTP.

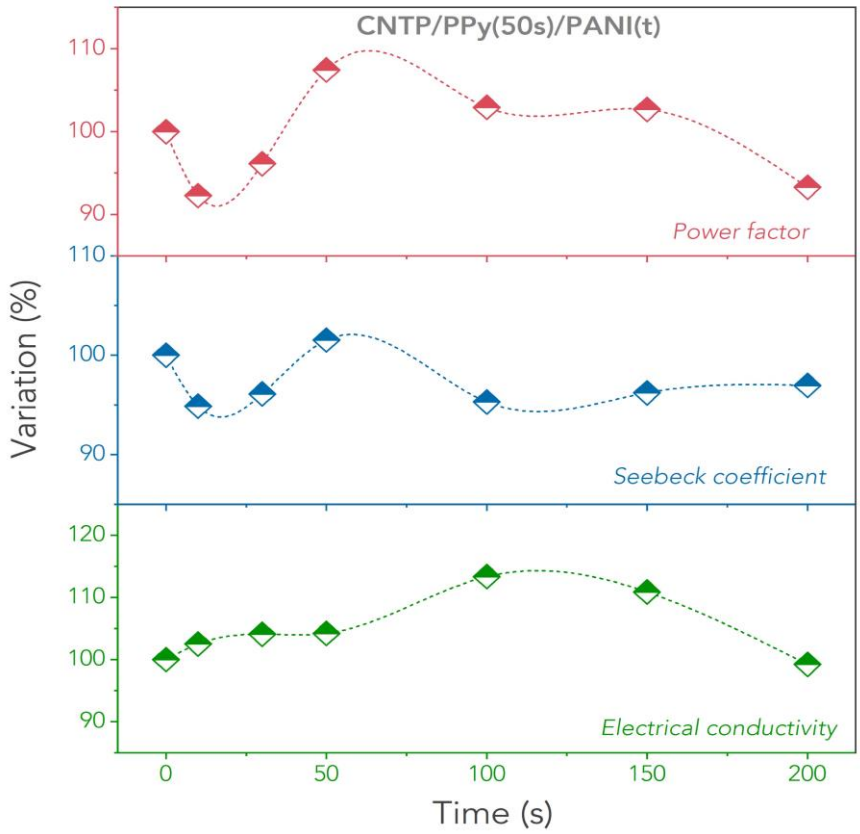

Figure S2. TE property variation as a funtion of electrochemical deposition time of PANI for the CNTP/P_y/P_a composites with the PPy deposition time fixed at 50 s. The reference data (100%) is extracted from CNTP/P_y.

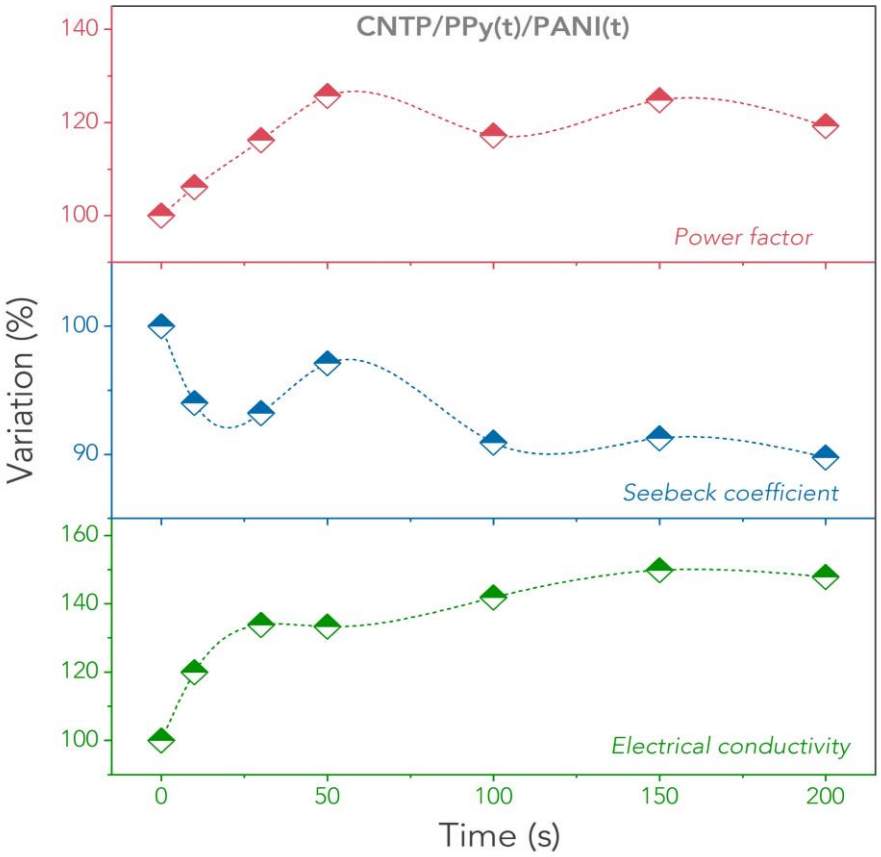

Figure S3. TE property variation as a funtion of electrochemical deposition time of PPy and PANI for the CNTP/P_y/P_a composites with identical PPy and PANI deposition time. The reference data (100%) is extracted from CNTP.

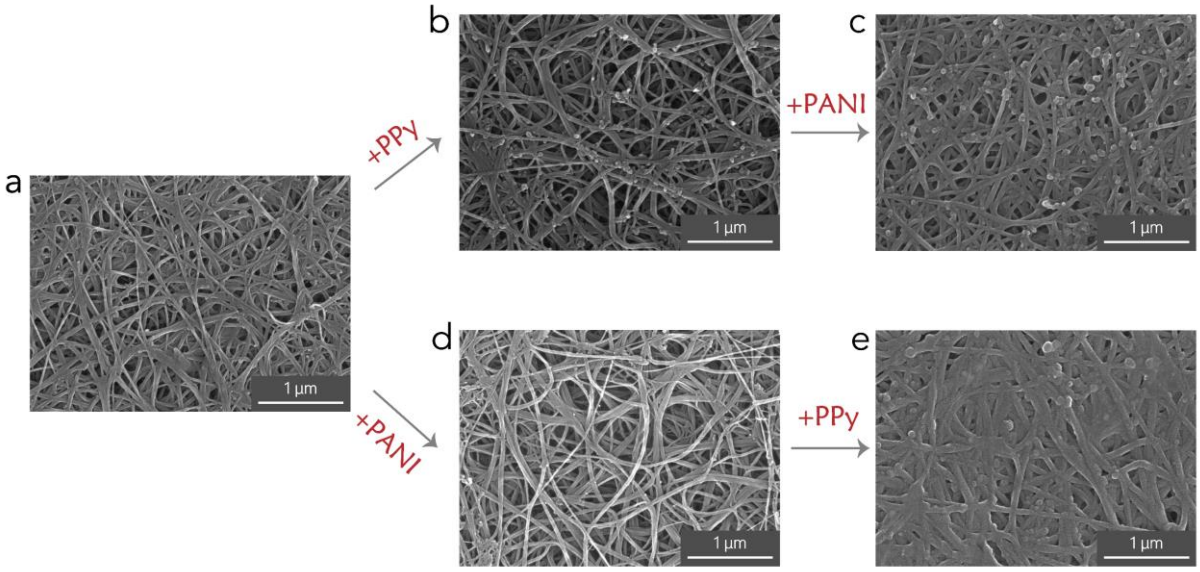

Figure S4. SEM images showing the morphology evolution of the nanocomposites during the preration process.

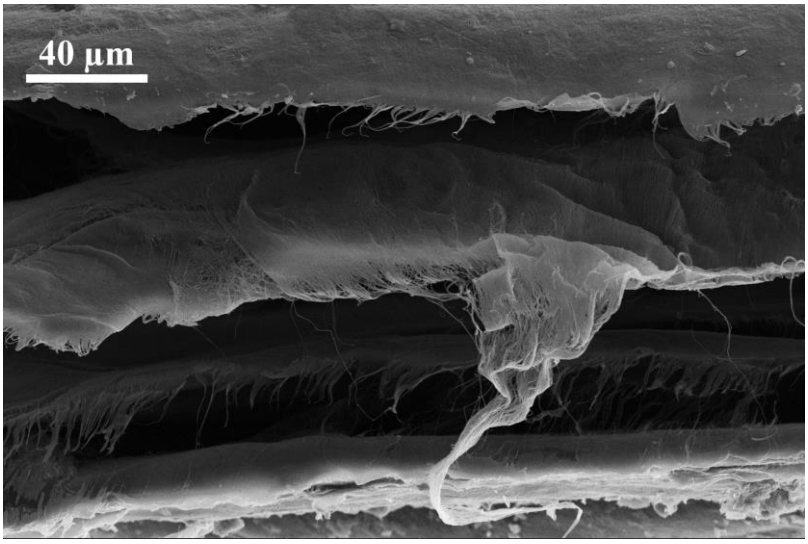

Figure S5. Cross-sectional SEM image of the CNTP/P_y/P_a nanocomposite film showing the multi-layer structure of the pristine CNTP and the deposited polymer on its surficial layer.

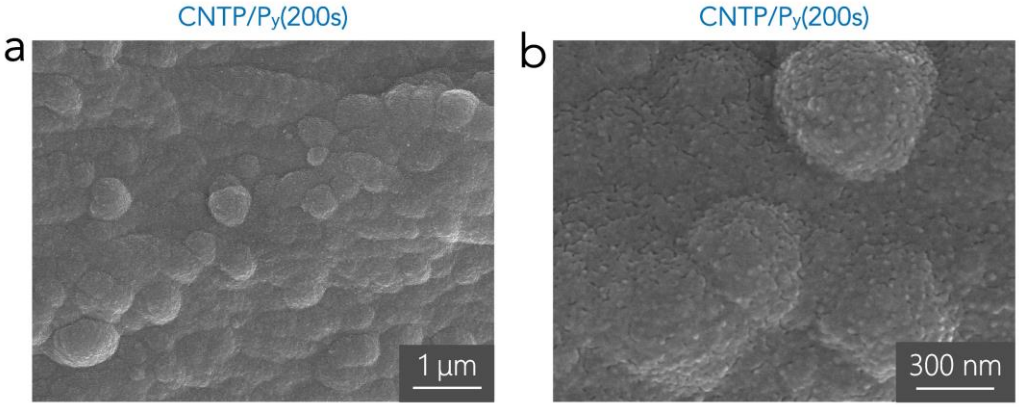

Figure S6. SEM images showing the morphology of the CNTP/P_y nanocomposites with the PPy deposition time of 200 s.

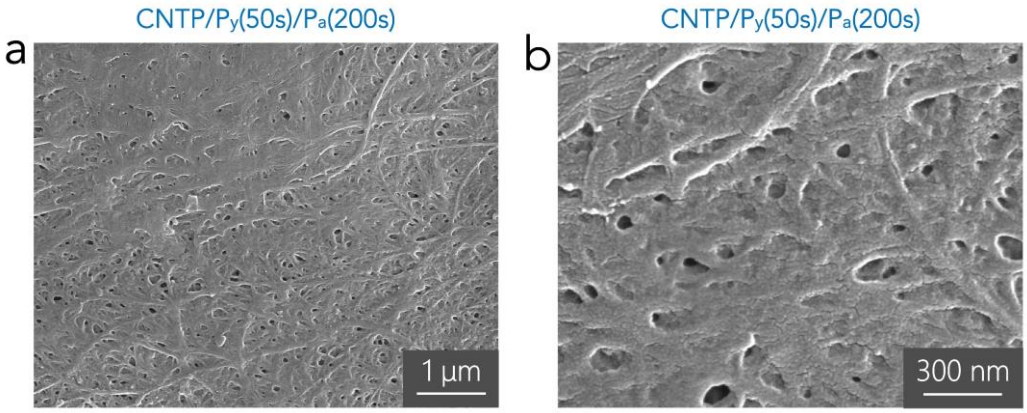

Figure S7. SEM images showing the morphology of the CNTP/P_y/P_a nanocomposites with the PPy deposition time of 50 s and the PANI deposition time of 200 s.

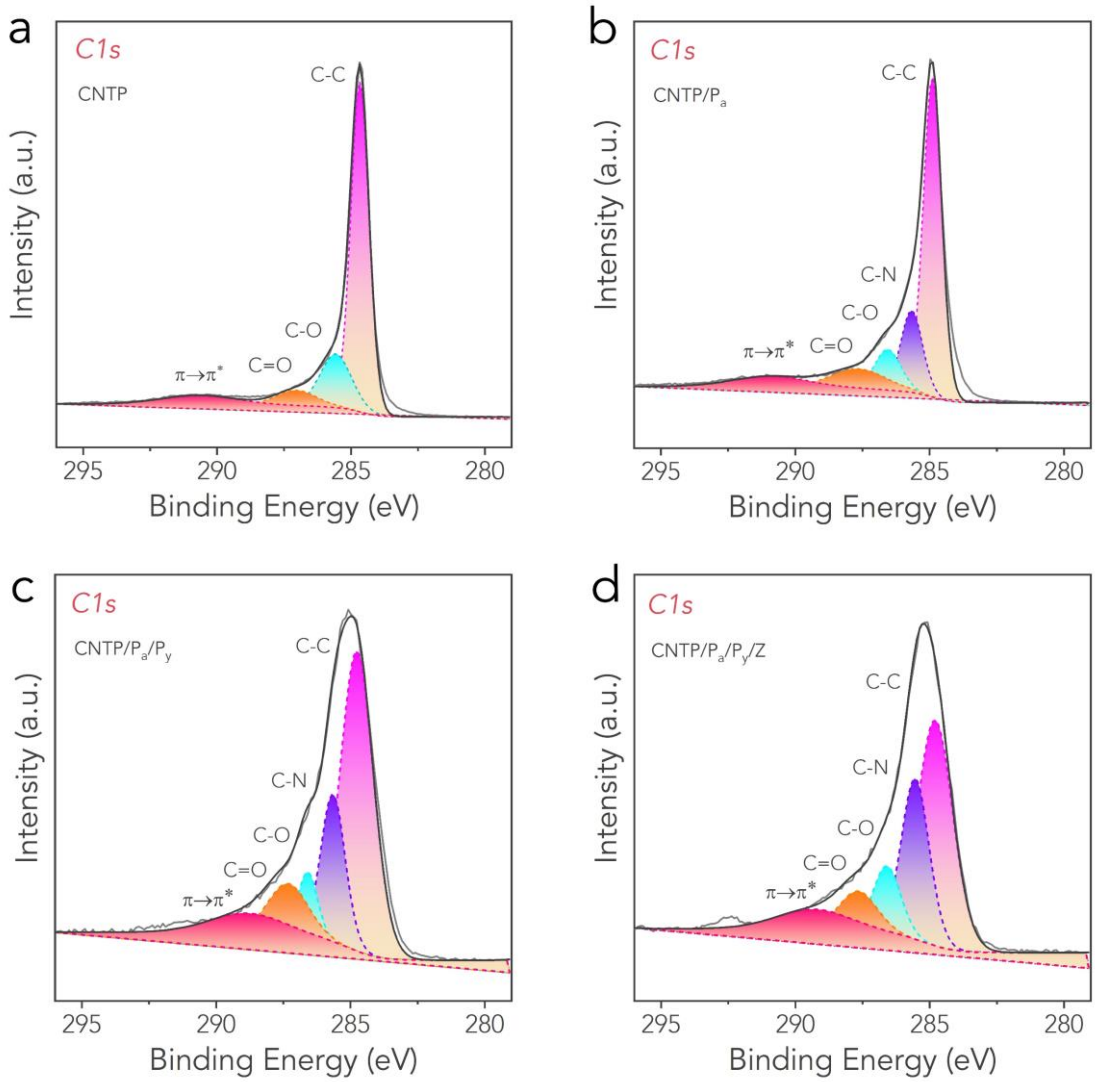

Figure S8. XPS C1s spectra of the (a) CNTP, (b) CNTP/P_a, (c) CNTP/P_a/P_y and (d) CNTP/P_a/P_y/Z nanocomposites.

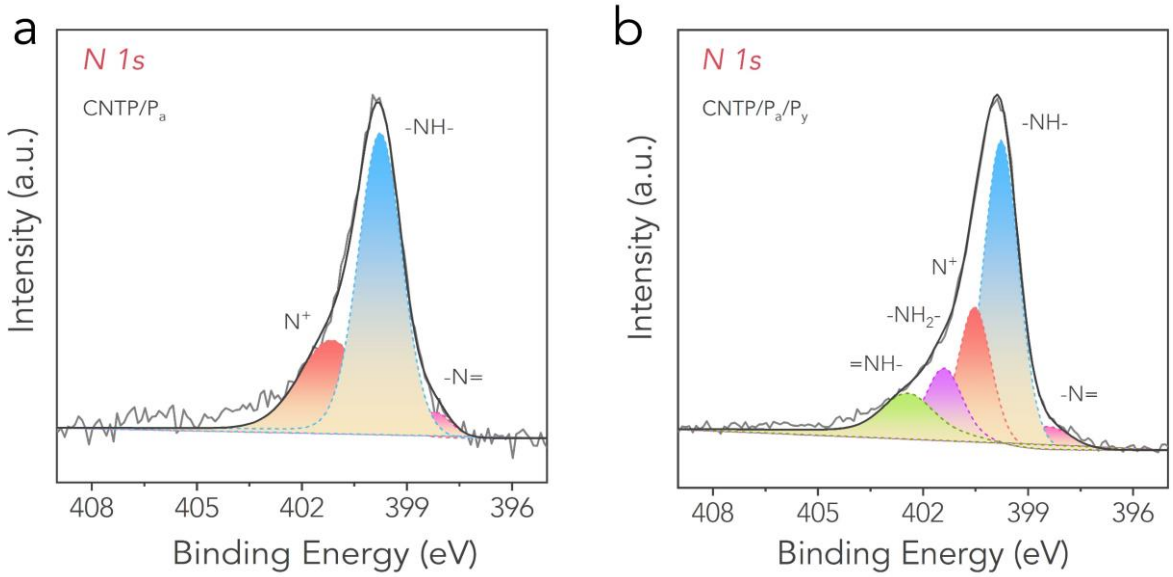

Figure S9. XPS N1s spectra of the (a) CNTP/P_a and (b) CNTP/P_a/P_y nanocomposites.

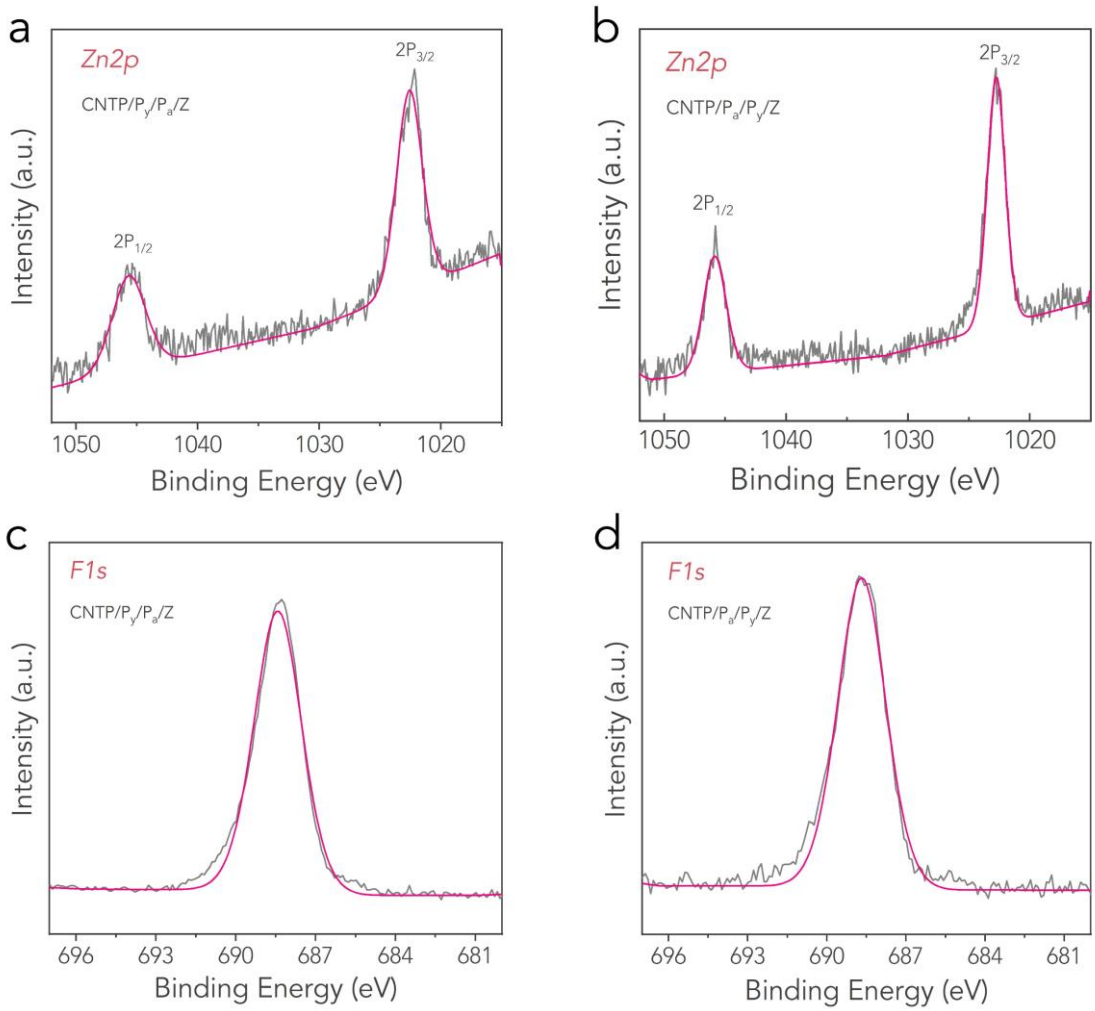

Figure S10. XPS Zn2p spectra of the (a) CNTP/P_y/P_a/Z and (b) CNTP/P_a/P_y/Z nanocomposites. XPS F1s spectra of the (a) CNTP/P_y/P_a/Z and (b) CNTP/P_a/P_y/Z nanocomposites.

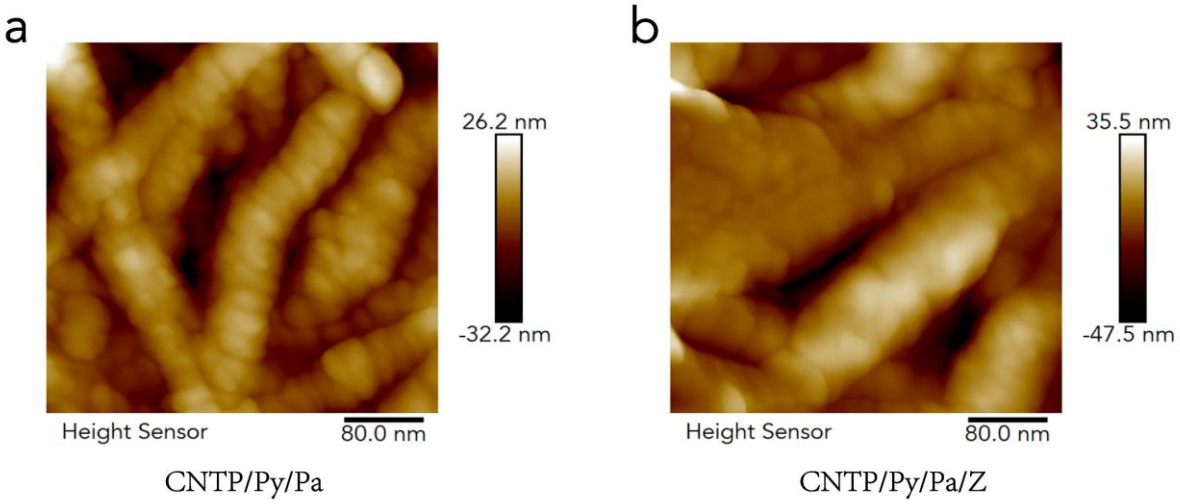

Figure S11. AFM images of the CNTP/P_y/P_a and CNTP/P_y/P_a/Z nanocomposites.

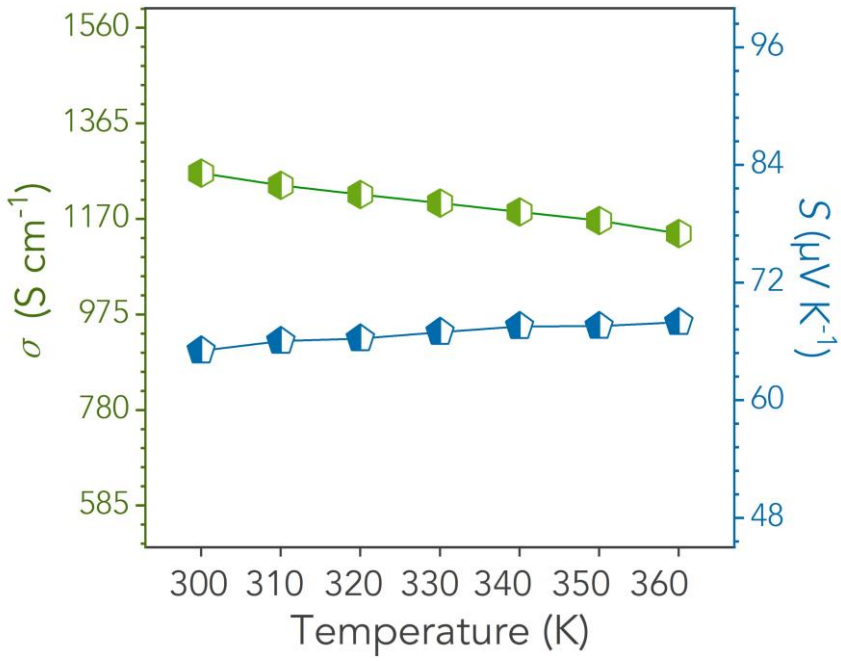

Figure S12. The electrical conductivity and the Seebeck coefficient variation of the CNTP/P_y/P_a/Z nanocomposite at elevated temperatures in air.

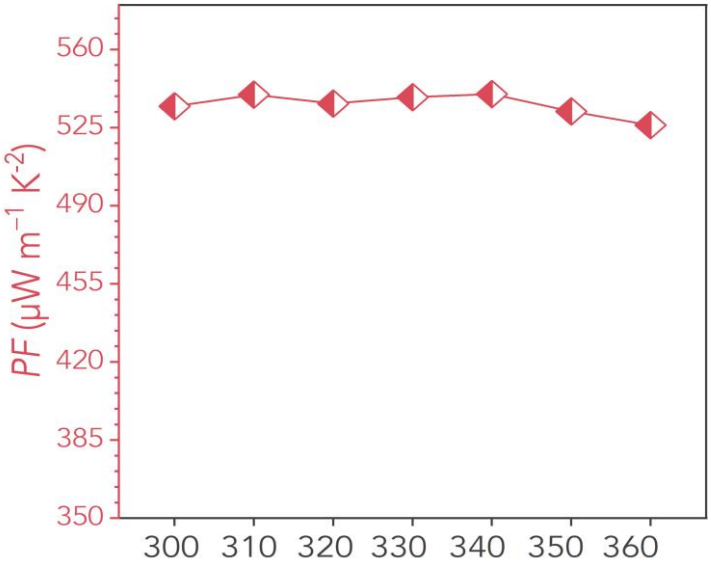

Figure S13. The power factor variation of the CNTP/P_y/P_a/Z nanocomposite at elevated temperatures in air.

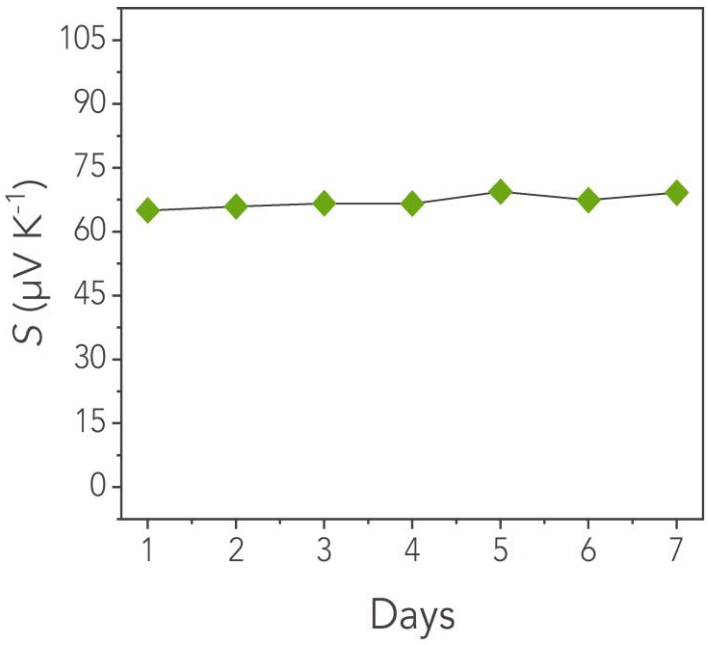

Figure S14. The thermopower variation of the CNTP/P_y/P_a/Z nanocomposite exposed to the ambient environment for successive 7 days.

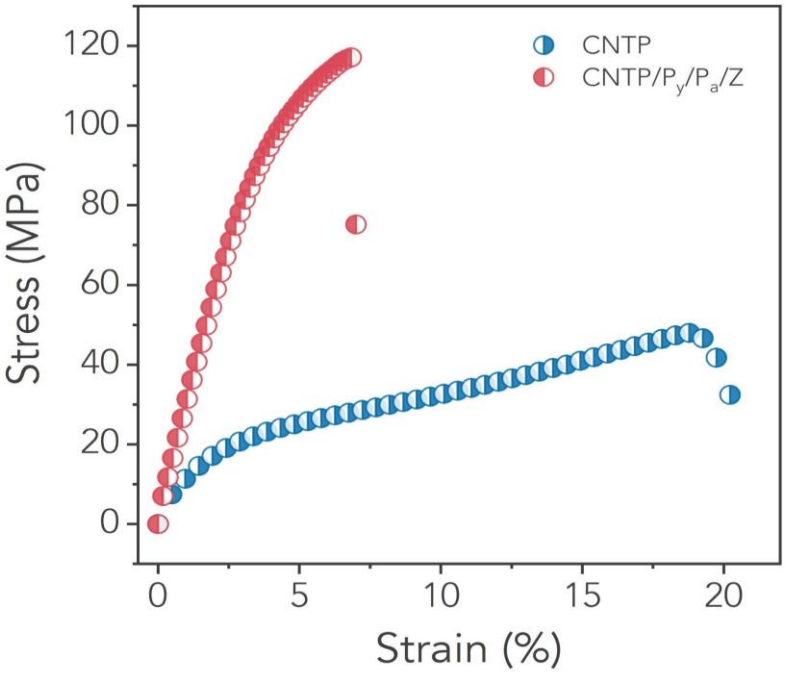

Figure S15. Stress-strain curves of the (a) CNTP and (b) CNTP/P_y/P_a/Z nanocomposites.

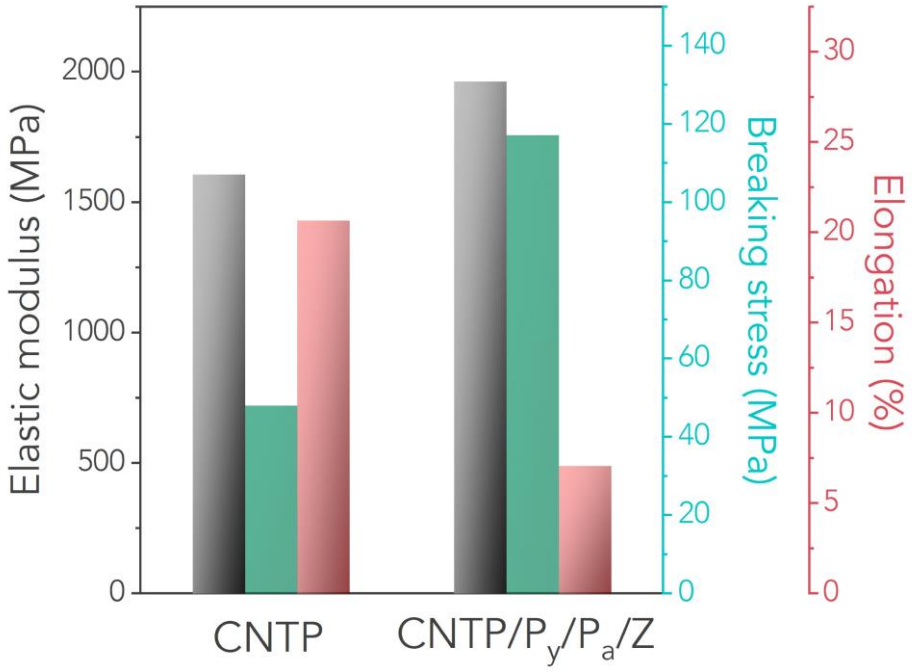

Figure S16. Mechanical property data of the (a) CNTP and (b) CNTP/P_y/P_a/Z nanocomposites.

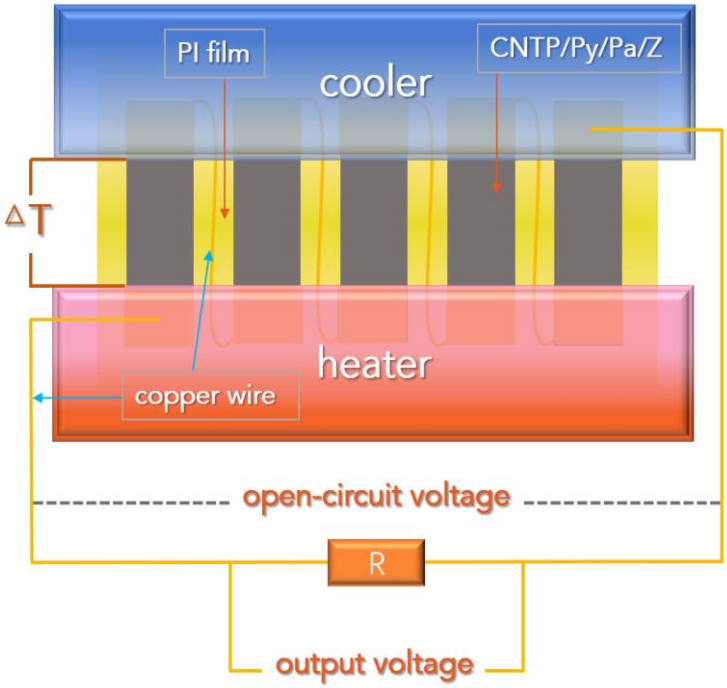

Figure S17. Illustration of the condiguration of the flexible TE device using CNTP/P_y/P_a/Z nanocomposite films as TE legs.

Figure S18. Time-depentant photos showing the OCVs of the flexible TE device when harvesting human body heat.